Frequency-induced structure transition of nematic electroconvection in twist cells

H. Bohatsch and R. Stannarius
Fakultät für Physik und Geowissenschaften, Universität Leipzig, Linnéstrasse 5, D-04103 Leipzig, Germany
(Received 15 October 1998; revised manuscript received 14 May 1999)

We investigate electroconvection of nematic liquid crystals in planar 90° twist cells in the dielectric regime. These cells provide competing boundary conditions for the nematic director at both electrodes. When the ratio of cell gap and roll width is not too small (in thin cells and at low frequencies), the convection rolls form along the director in the cell middle, which is diagonal to the anchoring directions. This is in accordance with known behavior in the conduction regime and with the assumption of a bulk instability (rolls traversing the cell). When the ratio of roll periodicity to cell gap is very small in the high-frequency range and the thick cells, a regular convection pattern sets in with wave vectors directed along the two alignment directions. We suggest the interpretation that two independent systems of convection rolls form localized near the electrode plates. It is very likely that a similar behavior occurs in nontwisted cells where it is difficult to identify experimentally. [S1063-651X(99)03611-9]

PACS number(s): 61.30.−v, 47.20.−k

I. INTRODUCTION

Electroconvection (EC) in nematics is among the most thoroughly studied dissipative pattern-forming systems. Since its first description by Williams and Kapustin [1], it has been investigated extensively in experiment and theory. A recent review can be found, for example, in [2]. Scientific interest has been revoked during recent years, for example with the discovery of abnormal rolls [3], new investigations of the homeotropic geometry [4–7], the study of defect turbulence and the onset of spatio-temporal chaos [8–11], the development of the weak electrolyte model [12], and progress in the description of chevron formation [13–15].

The convection mechanism is based on small periodic director fluctuations, which in connection with the anisotropic conductivity lead to the formation of a periodically modulated charge density in the sample plane. The interaction of these charges with the external electric field initiates a convective flow, which in turn augments the director deflection and drives the instability [16]. The dynamics of director and charge fields determine the character of the convection structures [17,18]. When the structures are driven with low-frequency ac electric fields, the sign of the charge density alternates with the electric field, and one deals with the well-analyzed conduction regime. The typical instabilities in this regime at onset are stationary or traveling roll cells perpendicular or oblique to the alignment axis at the surface. The width of the rolls is roughly equal to the cell gap. Above some characteristic frequency of the driving field, the cutoff, one finds the dielectric regime, which is also characterized by periodic rolls at the onset of the instability, at higher voltages by the formation of a chevron superstructure. The symmetries of charge and director deflection with respect to the polarity of the driving field are reversed; the director deflection alternates with the electric field. The spatial periodicity of the rolls decreases with increasing ac frequency, and is usually (cell gap >20 μm, frequency >100 Hz) much smaller than that of conductive rolls, often only a few micrometers. The onset voltage of dielectric convection rolls scales with the cell gap.

The standard theory [17–19] describes these dielectric convection structures as bulk instability. The wavelengths and critical electric field strengths are not sensitively cell thickness dependent. It is assumed that the rolls traverse the whole cell from electrode to electrode as shown in Fig. 1(a) (we will refer to them as bulk rolls). Since most of the experimental findings can be satisfactorily explained on the basis of this assumption, it is the established model of electroconvection in the dielectric regime. It seems, however, that from the experimental point of view it is difficult to prove this model directly, as is discussed below.

A different interpretation of some experimental results

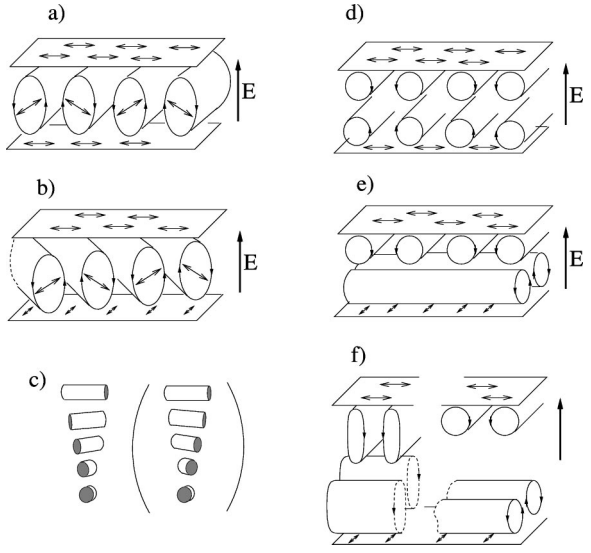

FIG. 1. Geometry of the nematic electroconvection in sandwich cells; arrows on the plates denote the surface anchoring (rubbing) direction. (a) Standard model in nontwisted cell; (b) standard model in a 90° twist cell; (c) director twist in the geometry of (b) and in brackets the opposite twist configuration which would lead to rolls rotated by 90°; (d) model of surface localized rolls in a nontwisted cell; (e) possible arrangement of surface localized rolls in a twist cell; (f) possible arrangement in thick cells, localized rolls at the electrodes (right) or elongated rolls in the cell (left).

was proposed a few years ago by Yamazaki, Kai, and coworkers [20,21]. The authors concluded that in their experiments dielectric rolls were localized near the electrodes only, as sketched in Fig. 1(d). We will use the term surface rolls for this structure. These conclusions were derived from two experiments. In [20], a sample cell with lateral electrodes was studied, with both electrode gap and cell gap of 100 μm. The optical image at low-frequency excitation showed roll textures which traversed the electrode gap. At high frequencies, the structures became localized in a thin region near the electrodes. A second experiment [21] was performed in a thin sandwich cell with conventional planar geometry; the structures were studied in transmitted light normal to the electrode plane. The authors observed striation patterns in two focus planes of the microscope separated by slightly less than the cell thickness,with an intermediate region where stripe patterns were absent. However, most of the experimental studies on dielectric patterns are obviously compatible with the standard description [17] and therefore the bulk model is generally accepted now. From an optical study of the transmission texture of a cell, it seems quite difficult to distinguish between both structure models.

Yamazaki *et al.* [21] have not analyzed the optical properties of a periodically deformed director field. Methods for the simulation of the optical characteristics of nematic convection rolls have been developed [22–27] and proved particularly useful for the description of rolls in the conduction regime. In that case, different virtual and real focal planes of the refraction pattern are found. If this is not considered in the interpretation of the optical images, the texture can pretend the existence of a complex height profile of the director pattern. In the dielectric regime, similar optical simulations give a qualitative explanation of the observed textures [28,29] but the simulations are useful only for small director deflections. The simulated textures are too indifferent with respect to the director profile along the cell normal.

The analysis of a side view of a cell with lateral electrodes as presented in [20] is not convincing evidence for localized structures in conventional sandwich cells. The geometry is more comparable to that of thin freely suspended films [30,31] where surface charges may play a nonnegligible role in the convection and where localized structures have also been observed.

We have set up an experiment which provides another insight in the structure of dielectric rolls. We will discuss the models mentioned above in the light of our experimental results, and describe some additional characteristic features of the observed patterns. Instead of cells with parallel anchoring, we use twisted cells where the surface anchoring of the director at upper and lower glass plate (rubbing directions) is planar but the alignment axis at the top electrode is perpendicular to that of the opposite electrode. In this geometry, both conduction and dielectric regimes are formed as in ordinary parallely rubbed planar cells. Previous electroconvection experiments with twisted cells have been reported in the literature [32–37], but the experiments have almost exclusively been restricted to the conduction regime. Because of the competing boundary conditions, the convection rolls choose a compromise between both surface orientations of the director if they are of the bulk type as in the conduction regime. The rolls are formed at $\pm 45°$ orientation with respect to the rubbing directions [see Fig. 1(b)]. In addition to the characteristic features found in nontwisted cells, rippled roll structures can appear in the twisted geometry, and thresholds and wavelengths of the rolls may differ slightly from those of nontwisted cells because of the additional elastic terms involved.

A similar behavior should be expected in the dielectric regime provided the rolls are of the bulk type. If, however, localized convection sets in near the electrodes, two independent convection layers should exist with different wavevector orientations [cf. Fig. 1(e)].

Since the wavelength of the roll pattern is strongly frequency dependent, the scan of a broad frequency range gives us the opportunity to control the wavelength versus cell gap ratio in two different ways, either by studying different cells or by varying the driving frequency of the electric field in one individual cell. A splitting of the convection rolls in the cell middle, possibly by the recombination of the charge fields, is more likely to occur in short wavelength rolls, i.e., at high ac frequencies.

II. EXPERIMENT

Our mesogenic material is the four-component mixture *Mischung 5* (Halle) of disubstituted phenyl-benzoates

with composition 1O-O6: 22.0%, 5O-O8: 30.3%, 6O-O7: 13.13%, 6-O4: 34.4%.

The mixture provides a nematic range from below room temperature to the clearing point at 70.5 °C, and a negative dielectric anisotropy $\epsilon_{\parallel}$-$\epsilon_{\perp}$. It has been studied in previous EC experiments (e.g., [15,28,29]).

We have used a commercial 90° twist cell with cell gap 14 μm from LINKAM (referred to as TN14) and self-assembled cells made with commercial glass plates (E.H.C.). The notation of these cells is TN39 (39.3 μm twisted), TN55 (54.5 μm twisted), TN102 (102 μm twisted), and N42 (42.3 μm nontwisted). The cell thickness has been determined by means of a UV/VIS spectrometer. All cells have transparent ITO electrodes and rubbed polyimide coating. Temperature control of the sample cells was achieved by a METTLER hot stage.

In some of the low-frequency experiments, the sample was observed orthoscopically in transmission with normally

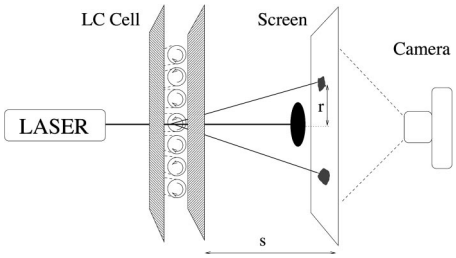

FIG. 2. Experiment laser scattering setup for the observation of short-wavelength structures; the distance between cell and screen is 132 mm. The central beamstop diameter is 20 mm, i.e., we exclude scattering from structures larger than $\approx 8\ \mu$m.

cident polarized white light using a JENAPOL-d microscope.

Most experiments in the high-frequency range have been performed with a Laser scattering setup (comparable techniques have been previously applied, e.g., in [38,39]). This method is particularly suitable to study the very short wavelength dielectric structures ($\geqslant 2\ \mu$m) where transmission microscopy fails. (The reason that the short wavelength is not observed with conventional transmission microscopy lies not primarily in the limited optical resolution but mainly in the large cell thickness to pattern wavelength ratio which smears out the transmission images.)

The sample is illuminated with a low power He-Ne laser (optical wavelength $\lambda_0 = 632.8$ nm) at normal incidence, and the diffraction pattern is recorded with a CCD video camera in a setup as shown in Fig. 2. This technique yields an image which has many features in common with a two-dimensional spatial Fourier transform of the optical transmission texture. Wavelengths and wave-vector orientations of the director tilt modulations in the convection structures can be directly extracted from the scattering peaks. Since the phase profile of the transmitted light at the upper boundary of the nematic is in rough approximation sinusoidal with half the periodicity of the director field modulation [24], we expect the largest scattering peaks at

$$r = \frac{\lambda_0}{\sqrt{\lambda^2 - \lambda_0^2}} s, \tag{1}$$

where s is the distance between the nematic cell and the screen, r is the displacement of the spot from the central beam on the screen, and λ gives the roll width (which is half the director period).

III. EXPERIMENTAL RESULTS AND DISCUSSION

The homogeneous ground state in the twist cell is twofold degenerate; the director can twist either by 90° or $-90°$ from the bottom to the top of the cell [Fig. 1(c)]. The final state of the director field in a cell is usually a monodomain, but often one finds long-time persistent domains of opposite twist, separated by a line defect (an $s = \frac{1}{2}$ twist disclination). In each domain, the director in the cell midplane is twisted either by $+45°$ or $-45°$ with respect to the anchoring direction at the lower plate. Consequently, there is also a degeneracy in the orientation of the convection rolls, but in general

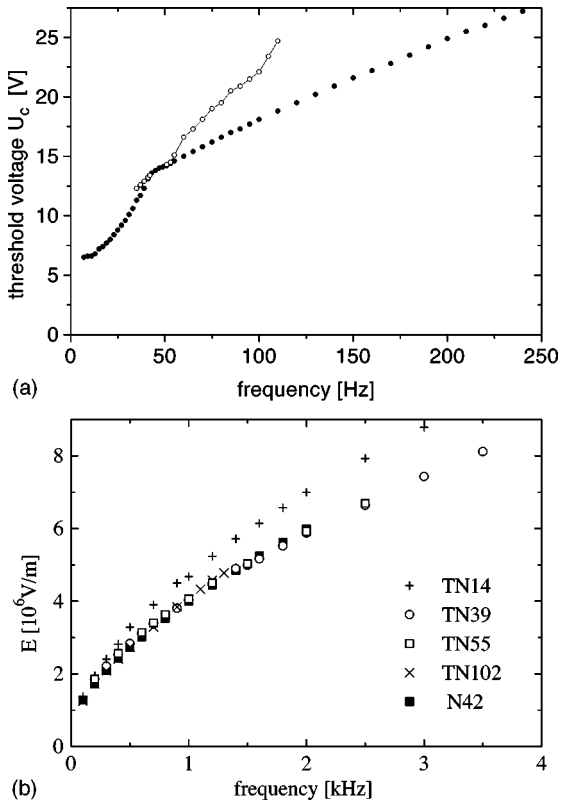

FIG. 3. (a) Onset threshold voltage for electroconvection in the twisted 14-μm cell at 50 °C. Near the cutoff $f_c = 41$ Hz, we observe a reappearance of conduction rolls above f_c and of dielectric rolls below f_c, above the voltages indicated by open circles. (b) Comparison of the onset electric-field strengths for twisted cells TN14, TN39, TN55, TN102, and the nontwisted reference cell N42.

the electroconvection structures are very similar to those in nontwisted cells.

Figure 3(a) shows the onset voltage of the convection pattern in the 14-μm twist cell at 50 °C. A peculiarity of this cell is that dielectric and conduction rolls coexist in the vicinity of $f_c = 41$ Hz. The open symbols above the first instability (dielectric rolls) mark a restabilization of static (conduction) rolls above f_c; similarly the short extension of the open symbols in the frequency range $f < f_c$ marks a restabilization of oscillatory (dielectric) rolls. The reason for this unusual behavior lies probably in the small cell thickness and low cutoff f_c which results in comparable wavelengths of both conduction and dielectric rolls near f_c.

A detailed experimental characterization and theoretical analysis of structures in the low-frequency conduction regime has been performed by Hertrich *et al.* [36,37]. Therefore, we will not go into the details of conductive rolls here but deal exclusively with the dielectric regime. Figure 3(b) compares the onset field strengths for dielectric rolls of the cells investigated. All cells behave quite similarly when the threshold voltage U_C is scaled with the cell gap d. In particular, the threshold curve of the twisted cell TN39 coincides with that of the nontwisted cell N42, which is included for comparison. The threshold field strength for the TN14 cell is slightly increased with respect to the other cells, presumably because of the additional elastic contributions of the stronger twist.

Figure 4 shows the frequency dependence of the pattern-

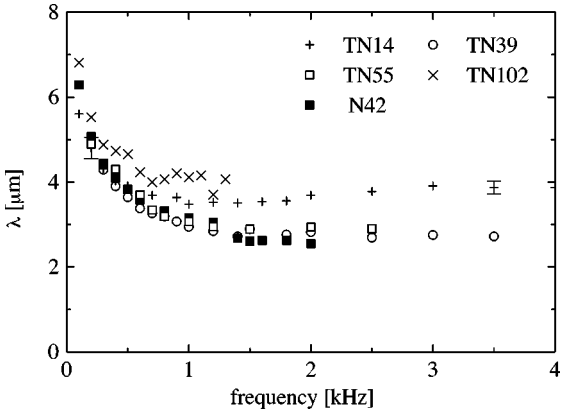

FIG. 4. ''Optical'' periodicity λ in the different cells extracted from the laser diffraction spots.

period λ (half period of the director tilt, width of the convection rolls) extracted from the laser scattering images. All cells show a common behavior, the roll period decreases with frequency, and it seems that in all cases some saturation plateau is reached at high frequencies. Within standard theory, the wavelength should continuously decrease with frequency. Since the accuracy of the wavelengths determined from the diffraction images improves with decreasing wavelength, the deviations from the expected $f^{-1/2}$ law cannot be attributed to experimental inaccuracies. Probably, some of the suppositions made by theory break down in the respective parameter range. For example, theory makes certain assumptions about the relation between the charge-carrier motion and the material flow in the cell: the velocity of charges in the electric field and that of the liquid-crystal molecules are usually set equal. However, more systematic experiments would be required to propose suitable modifications of theory.

Figures 5–7 represent some typical optical textures observed in the dielectric regime. The image in Fig. 5 shows a roll pattern near the threshold voltage. The roll orientation is diagonal to the rubbing directions. Two domains corresponding to oppositely twisted director configurations [cf. Fig. 1(c)] are separated by the disclination line in the middle of the image. A typical chevron texture in the TN14 cell is shown in Fig. 6. When the chevron defect chains start to move, material flow sets in along these chains (marked by arrows in Fig. 6) and the domain boundaries are deformed by the flow field. The convection rolls are very small already and not well resolved in the reproduction of the microscopic picture, but since we have recorded the image with circularly polarized light [40], the chevron stripes are seen by alternation dark and bright bands [29,15].

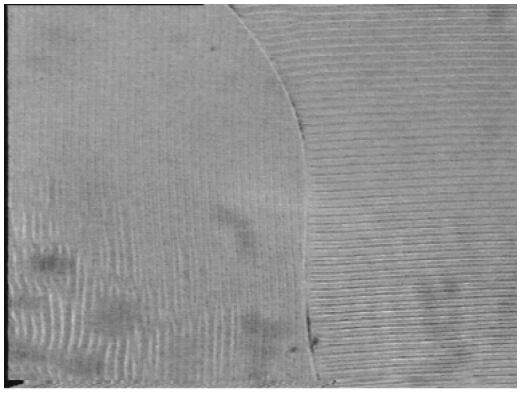

FIG. 5. Microscopic image of dielectric rolls in a 14-μm twist cell, $T=29.5°$, $f=15$ Hz, $f_c=14$ Hz, $U=14.86$ V, $U_C=12.4$ V. The rolls are diagonal to the rubbing directions (crossed bars). Two domains [cf. Fig. 1(c)] are separated by a defect line. In the lower left part the beginning restabilization of conduction rolls is seen. Image size 400×300 μm.

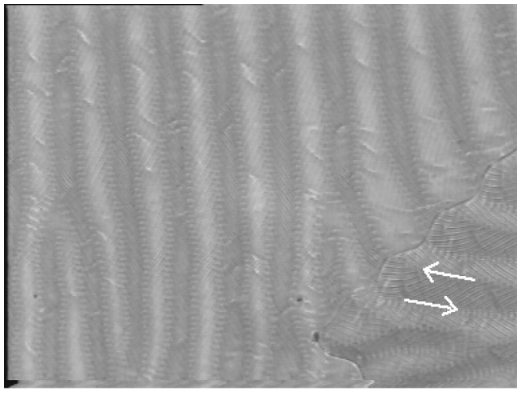

FIG. 6. Same as in Fig. 5, $f=70$ Hz, $U=31.5$ V. The defect line between the two domains is deformed by material flow in the defect chains (arrows). The convection rolls are hardly observable, therefore we have visualized the chevron pattern with circularly polarized light.

At higher voltages, the flow along the defect chains is strong enough to overcome the line tension of the domain boundaries. Islands are torn out of the adjacent domain and carried as wormlike structures with the flow; they move along the chevron stripes. Their shape is elongated in the direction of motion. The director field inside these worms is oppositely twisted with respect to the surrounding material, therefore they are enclosed by a disclination line in the director field. They keep their shape and constant length during the motion but dissolve when they reach a defect in the chevron stripes (in that case the flow at the front stops while the tail of the worms moves on and extinguishes the domain).

From Figs. 5–7 we draw the conclusion that the dielectric

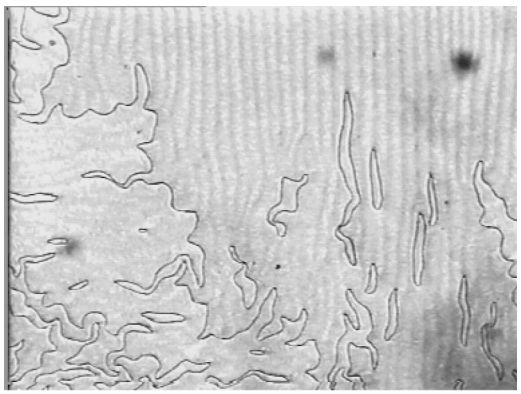

FIG. 7. Same cell as in the previous figures, $f=500$ Hz, $U=80.37$ V, image dimensions 600×450 μm. The dark and bright lines correspond to chevron stripes visualized by means of circularly polarized light. Worms (domains with opposite sense of twist than the surrounding material) move along the defect chains.

convection structures in the 14-μm cell form a compromise between the surface anchoring directions on both glass plates of the sandwich cell. Another key observation is that we observe two focal planes of the microscopic image, one near the upper glass plate and a second near the lower glass plate, and in both, directions of the stripes they coincide. We have taken microscopic images of the 14-μm twist cell up to 10-kHz driving frequency. At high frequencies (>1 kHz), it was not possible to resolve the convection rolls but the chevron pattern was visible. The direction of the chevron stripes remained along the cell diagonal at all frequencies.

Since the primary instability is the dielectric rolls, we have focused our further attention on these structures. With the laser scattering technique we have determined their orientations in the twisted cells over a broad frequency range. A reference system (x,y) is chosen diagonal to the rubbing directions of the cell, and the deviation angle of the wave vector of the rolls from the y axis is denoted by α. The diffraction pattern at the onset of convection in the TN14 cell is shown in Fig. 8(a). In the laser spot, the sample is monodomain here and the image consists of two narrow reflexes. The wave-vector orientation is $\alpha=0$. After the voltage is increased [Fig. 8(b)], each of the reflexes splits into two slightly broadened spots arranged symmetrically with respect to the y axis. This is characteristic of the modulation of the wave-vector field in the chevron pattern. The average orientation of the convection rolls in the chevrons can easily be extracted.

A quantitative presentation is given in Fig. 9. Since the reflexes of the different in-plane wave-vector orientations in each image always below to the same wavelength, they are located on a circle around the central beam. Therefore, we have reduced the data to the intensity profile on a ring around the central spot, which intersects all reflexes. In Fig. 8(b), the dashed circle indicates where such an intensity profile would be taken in the image. Figure 9(a) shows the change of this profile during the transition from normal rolls to chevrons. At low voltages above U_C the profile shows two narrow peaks at $\alpha=0$ $(180°)$. Each maximum splits into two sharp reflexes when the chevrons are formed. The positions of the peaks as a function of the driving voltage [expressed by the control parameter $\epsilon=(U/U_C)^2-1$] are collected in Fig. 10. For each image we show the average of the southwest and northeast spots as well as that of the southeast and northwest reflexes. Because the peaks lie symmetric with respect to the y axis, we depict the absolute values of α.

In the 14-μm cell, we find an onset orientation of $\alpha=0°$ at all frequencies up to several kHz. The instability of the ground state is towards normal rolls along the diagonal. The transition to chevrons at 100 Hz starts near $\epsilon_{ch}=0.62$ and at 7 kHz near $\epsilon_{ch}=0.28$. At all intermediate frequencies, the same qualitative behavior is found, with a continuous shift of the threshold ϵ_{ch} for chevron formation.

The scattering reflexes of the thicker cells behave qualitatively different from those of the TN14 cell. The orientations of the scattering reflexes in the TN39 cell as functions of the control parameter are presented in Fig. 11. The figure shows the characteristics of the convection rolls at four different frequencies of the driving field. Depending upon frequency, we find two different scenarios. Only in the low-frequency measurements up to 300 Hz does the cell behave like TN14. The rolls are formed along the diagonals, α remains zero at least for $\epsilon<0.06$, and at higher voltages the reflexes split, presumably because of chevron formation again. In a broad frequency range around 1 kHz, we no longer find sharp reflexes along the diagonals. Instead, two pairs of reflexes appear already at the onset of convection. These reflexes are broad, smeared out, and fluctuating; their maximum is located near $\pm 10°$. Their orientations rapidly shift to higher angles with increasing voltage. At frequencies above that transition range (above ≈ 1500 Hz), the reflexes at onset are sharper again, but they appear now near the $\alpha=\pm 45°$ orientations, corresponding to wave vectors along the director easy axes at the glass plates. This is best seen in the intensity profiles of Fig. 9(b). The intensity of the 45° peaks increases continuously with ϵ while the orientation remains nearly parallel to the surface alignment axes. The data for 3500 Hz in Fig. 11 are representative for the high-frequency behavior.

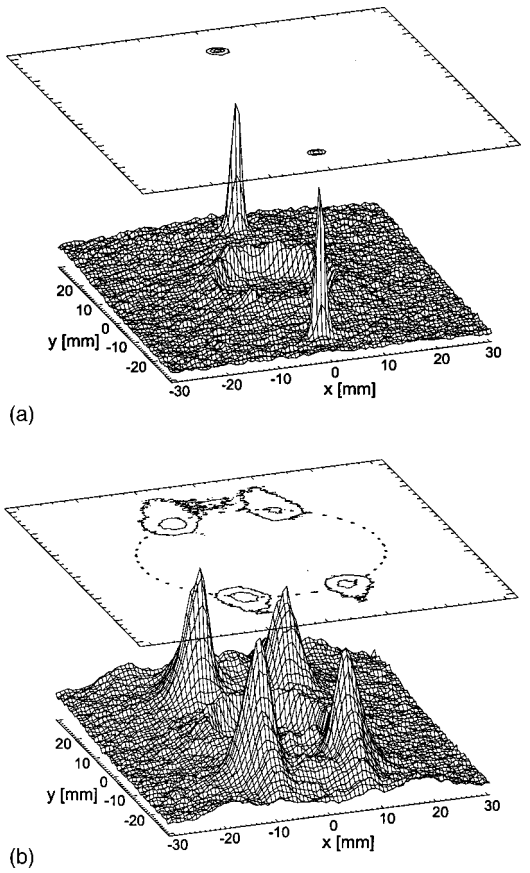

FIG. 8. Diffraction profile of a He-Ne laser (632.8 nm) beam in twist cells. The central beam stop is 2 cm in diameter. (a) TN14 $U=66.5$ V ($\epsilon=0.031$), 1000 Hz: $\alpha=0$, normal rolls at the onset of electroconvection, diagonal to the rubbing directions; (b) TN14 $U=86.5$ V ($\epsilon=0.744$), 1000 Hz: $\alpha=\pm 26°$, chevrons diagonal to the rubbing directions. The dashed circle sketches where the intensity profiles in Fig. 9 were obtained.

With further increasing cell thickness, the qualitative picture remains the same, but the transition from the low-frequency to high-frequency characteristics occurs at lower frequencies. In Fig. 12 we show the data of a 54.5-μm cell at 600 Hz (fluctuating smeared reflexes with small α at $\epsilon=0$) and 800 Hz (onset already near 35°). The transition appears

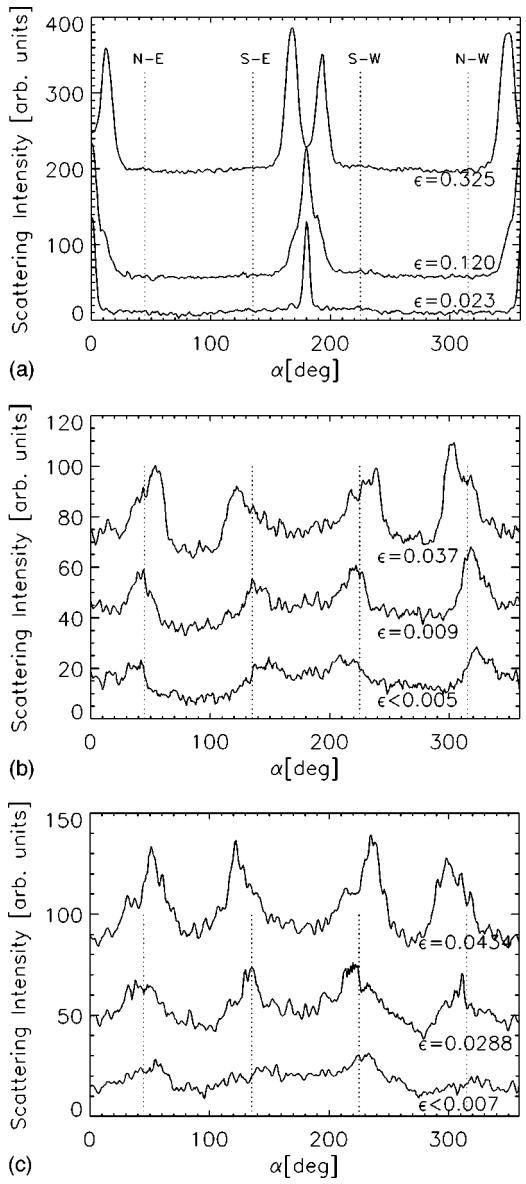

FIG. 9. Intensity profiles of the scattering images on a circle around the central beam [constant r in Eq. (1)] at the positions of the maximum reflexes; see the dashed line in Fig. 8(b). (a) TN14 at 1400 Hz, transition from normal rolls to chevrons; (b) TN39 at 1800 Hz, rolls aligned to the rubbing directions; (c) TN102 at 500 Hz, rolls aligned to the rubbing directions.

now in a frequency range around 600 Hz. Again, at high frequencies (>1 kHz) the regular pattern sets in nearly parallel to the rubbing directions $\pm 45°$, and at low frequencies (<300 Hz) the convection starts with $\alpha=0$.

The orientations of the reflexes in the thick TN102 cell are presented in Fig. 13. Here, we find no sharp reflexes at all for low frequencies. At 100 Hz, there are some broad, diffuse spots near $\alpha=0$ which rapidly drift to higher α with increasing ϵ, but already at 400 Hz the transition to the high-frequency characteristics is complete. The images consist of four spots localized near $\pm 45°$; the reflexes are not as sharp as in the thin cell but are well defined [see Fig. 9(c)].

At first glance, the profiles in Figs. 9(b) and 9(c) are very similar to those of a chevron texture where the deflection of the rolls is incidentally $\pm 45°$. Hence one cannot decide immediately from one scattering image whether the high-frequency patterns originates (a) from a lateral modulation of the wave vector, a zigzag arrangement of rolls like in a chevron structure; (b) a multidomain sample with wave vectors arranged along one of the rubbing directions in each individual domain; or (c) a superposition of convection rolls at the upper and lower electrodes with wave vectors along the corresponding director surface alignment.

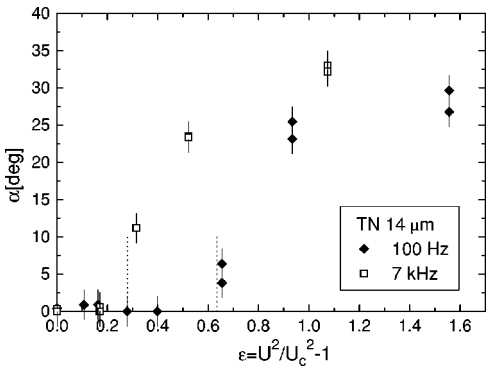

FIG. 10. Change of the angle α (absolute value) between the diagonal and the wave vector of the convection rolls with driving voltage in cell TN14 at 100 Hz and 7 kHz. There is no qualitative change over the whole frequency range. The patern starts with normal rolls. With the formation of chevrons, the scattering reflex splits, clockwise and counterclockwise rotated sets of rolls appear, deflected by the same angle in opposite directions.

It is reasonable to dismiss the first two interpretations. In the experiments, the four spots always have comparable intensities. In a multidomain sample it would be pure coincidence if both domains always shared equal portions of the measuring spot. Moreover, we have carefully established that the orientation does not jump near the threshold; α is approximately 45° already at the onset of the instability. While the intensity of the peaks increases with ϵ, the orientation is nearly preserved. This is strong evidence against the chevron interpretation. Such a structure always appears as a second-

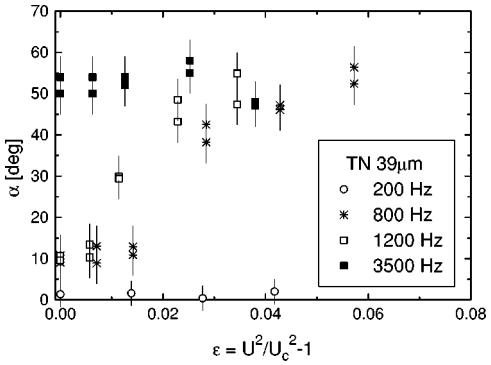

FIG. 11. Change of the angle α between the cell diagonal and the wave vector of the convection rolls for cell TN39 between 200 and 3500 Hz. At 200 Hz, the wave vector is along the cell diagonals as in the TN14 cell. Between 800 and 1200 Hz, the pattern becomes rather diffuse and fluctuating at onset; the wave vector clearly deviates from $\alpha=0$. With increasing frequency it stabilizes again. Above 3500 Hz, the reflexes indicate wave vectors along the rubbing directions at the onset. We interpret these images as the transition from bulk rolls ($\alpha=0$ at onset) to surface rolls ($\alpha\approx 45°$ at onset).

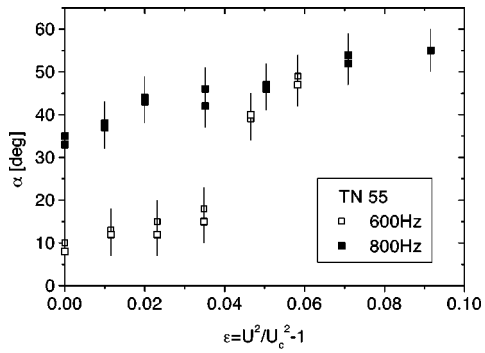

FIG. 12. Transition from bulk rolls (roiented along the diagonals) to surface rolls (oriented parallel to the director at the surfaces) in the TN55 cell controlled by the frequency of the driving field. Data for two frequencies in the transition range are shown.

ary instability with wave-vector deflections being strongly ϵ-dependent near the onset.

When the voltage is further increased, the reflexes become gradually broader and the orientation changes gradually towards higher α. An interpretation of this behavior is beyond the scope of this work. A reorientation of the convection rolls with respect to the surface alignment with increasing voltages is typical in electroconvection, and since the symmetry is broken by the imposed twist here, it is not surprising that this reorientation leads to a shift instead of the splitting of the scattering peak. It is important to note that with increasing cell thickness, we also observe a large increase of diffuse scattering around the central beam, corresponding to wavelengths >10 μm, in particular at higher frequencies.

We propose that the experimental observations are interpreted with assumption (c). A system of two roll textures with wave vectors nearly perpendicular to each other is formed in the cell. From their orientations it is reasonable to conclude that these rolls are positioned near the electrode plates. Since the lateral width of the observed director structures is more than one order of magnitude smaller than the cell gap, the convection rolls probably do not extend much more than their lateral extension into the depth of the cell [right image in Fig. 1(f)]. The middle of the cell is in a

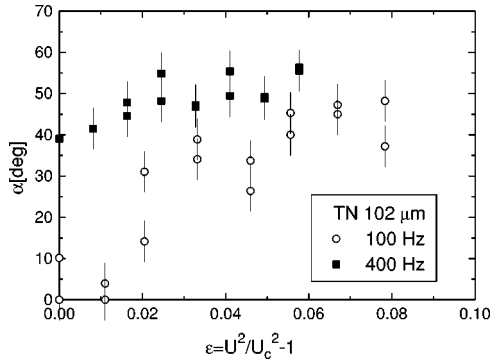

FIG. 13. Same as in Figs. 11 and 12 for cell TN102 at 100 and 400 Hz. At 100 Hz, the pattern is rather diffuse and fluctuating; with increasing frequency it stabilizes. Above 400 Hz, there are only minor changes in the characteristics of $\alpha(\epsilon)$ for small ϵ; the pattern starts with wave vectors nearly parallel to the rubbing directions.

structureless convection state. The strong increase of long-wavelength scattering, in particular in the TN102 cell, is a consequence of disordered director fluctuations in the material between the two ordered convection layers.

In order to understand the diffraction images observed, it is important to note that the diffraction efficiency of the phase grating established by the director field in the convection rolls is low, only a few percent. After passing the first layer of convection rolls, most of the intensity is still contained in the primary beam, and two diffracted beams appear, corresponding to the wave vector q_1 at the bottom electrode. When the light passes the second system of rolls at the opposite glass plate, the primary beam is diffracted again and two additional spots occur, corresponding to the wave vector q_2 at the top electrode. The reflexes corresponding to $q_1 \pm q_2$ have much lower amplitudes. They are consequently not observable in the experiment.

Within our simple model, we can explain the diffraction images, but the experiment does not provide direct information on the depth of the rolls. An indirect argument can be derived from the existence of bulk structures in the 14-μm cell and the loss of bulk behavior in the 39-μm cell, which indicates that the depth of the rolls in thick cells, in a rough estimation, does not exceed ≈ 10 μm. It is reasonable to assume that the ratio of pattern wavelength versus cell gap plays an essential role in the transition from bulk rolls in thin cells to surface rolls in thick cells. This argument also explains the frequency dependence, which is in fact a wavelength dependence. If we relate the cell thicknesses to the widths of the convection rolls in the transition range, we find the ratios of about 1:14 in TN39, 1:17 in TN55, and 1:20 in TN102. This gives a rough estimate of the conditions at which a breakdown of the bulk properties of dielectric rolls can be expected in other cells.

The behavior in the transition range is not easily understood. The experiments show that there is not an abrupt transition from bulk rolls to surface rolls at some critical ratio of roll width to cell thickness. Instead, the rolls start to deviate continuously from $\alpha=0$, with nearly equal contributions from the two opposite orientations. Our interpretation is as follows: As long as the two roll systems are still in contact in the cell middle, there will be a considerable correlation of the director and flow fields, with an increasing number of defects arising when the wave vectors at both sides start to differ. This causes not only the deviation from $\alpha=0$, but also a broadening of the reflexes on a ring around the central beam. Even when the flow field of both convection layers is completely decoupled, there will still be a coupling via the twist deformation of the director field, and the rolls have to form a compromise between surface orientation and director in the cell middle. Only after the separation of the two roll systems has become large enough with increasing frequency (i.e., decreasing λ) can two independent layers of convection rolls exist. Between these layers, the director will be in a more or less disordered state with structureless convective flow, causing an increasing intensity of small-angle scattering.

IV. SUMMARY

We have determined the onset thresholds, wavelengths, and wave-vector orientations of electroconvection rolls in the

dielectric regime in 90° twisted nematic cells. The patterns are quite similar to those observed in nontwisted cells. One particular feature of the convection rolls which cannot be understood within standard theory is the frequency dependence of the wavelength. It should be a continuously decreasing $q/\sqrt{f}$ function of frequency. In the experiments, we find a saturation at wavelengths above 2 μm. Further experiments with nontwisted samples are in progress to study this discrepancy in more detail.

A dramatic change is observed between the orientations of the patterns generated in thin (14 μm) and thick ($\geqslant$39 μm) cells. In the 14-μm cell, the orientation of the convection rolls at onset is along the diagonal between the rubbing directions. As in the conduction regime, the convection chooses a compromise between both boundary conditions at the opposite cell planes. With increasing ratio of cell gap versus roll width, which can be controlled either by using cells of different gap or by varying the driving frequency, there is a structural transition to rolls with wave vectors along the rubbing directions of the cell. Obviously, this orientation is imposed by the boundary conditions for the director field at the glass plates. This is evidence that at sufficiently high ratios of cell gap to roll width, a localized convection near the cell plates exists, which is independent of the convection field in the cell middle and at the opposite electrode, i.e., the regular electroconvection rolls are restricted to the surfaces and the ordered convection breaks down in the cell middle. For thick cells and/or high frequencies, our observations support the model proposed by Kai *et al.* [21,20]. It seems that the rolls extend at maximum $\approx$10 μm from the boundaries into the cell. Their depth is presumably not significantly larger than the lateral width.

It is reasonable to assume that the effects reported here for twist geometry are not a peculiar feature of twisted nematic cells but that the conclusions are adequately valid in the geometry of parallely rubbed cells. We haven to found an experimental confirmation of this hypothesis yet. However, one should take into consideration that the effect of localization is most pronounced in the thick 102-μm cell in which the twist is much smaller than in the 14-μm cell, and which is much more comparable to a nontwisted planar geometry than the thin twist cell.

ACKNOWLEDGMENTS

We acknowledgment fruitful discussions with L. Kramer (Bayreuth), H. Schüring, and M. Grigutsch. This study was supported by the DFG with Grant No. STA 425/3.

[1] R. Williams, J. Chem. Phys. **39**, 384 (1963); A. P. Kapustin and L. K. Vistin, Kristallografiya **10**, 118 (1965) [Sov. Phys. Crystallogr. **10**, 95 (1965)].

[2] L. Kramer and W. Pesch, Annu. Rev. Fluid Mech. **17**, 515 (1995); L. Kramer and W. Pesch, *Electrohydrodynamic Instabilities in Nematic Liquid Crystals*, in *Pattern Formation in Liquid Crystals*, edited by A. Buka and L. Kramer (Springer, New York, 1995), and references therein; S. Kai and W. Zimmermann, Suppl. Prog. Theor. Phys. **99**, 458 (1989); L. Kramer and W. Pesch, Annu. Rev. Fluid Mech. **17**, 515 (1995).

[3] E. Plaut, W. Decker, A. Rossberg, L. Kramer, W. Pesch, A. Belaidi, and R. Ribotta, Phys. Rev. Lett. **79**, 2367 (1997); S. Rudroff *et al.*, *ibid.* (to be published).

[4] H. Richter, N. Klöpper, A. Hertrich, and A. Buka, Europhys. Lett. **30**, 37 (1995).

[5] P. Tóth, A. Buka, J. Peinke, and L. Kramer, Phys. Rev. E **58**, 1983 (1998).

[6] S. Kai, K. Hayashi, and Y. Hidaka, J. Phys. Chem. **100**, 19 007 (1996).

[7] Y. Hidaka, Jong-Hoon Huh, K. Hayashi, M. I. Tribelsky, and S. Kai, J. Phys. Soc. Jpn. **66**, 3329 (1997); Y. Hidaka, Jong-Hoon Huh, K. Hayashi, S. Kai, and M. I. Tribelsky, Phys. Rev. E **56**, R6256 (1997).

[8] M. Dennin, G. Ahlers, and D. S. Cannell, Science **272**, 388 (1996).

[9] M. Dennin, D. S. Cannell, and G. Ahlers, Phys. Rev. E **57**, 638 (1997).

[10] I. Rehberg, S. Rasenat, V. Steinberg, and V. Steinberg, Phys. Rev. Lett. **62**, 756 (1989).

[11] S. Rudroff and I. Rehberg, Phys. Rev. E **55**, 2742 (1997).

[12] M. Treiber and L. Kramer, Mol. Cryst. Liq. Cryst. Sci. Technol., Sect. A **261**, 303 (1995); Martin Treiber and L. Kramer, Phys. Rev. E **58**, 1973 (1998).

[13] M. Scheuring, L. Kramer, and J. Peinke, Phys. Rev. E **58**, 2018 (1998).

[14] A. G. Rossberg, dissertation, University of Bayreuth (1998); A. G. Rossberg and L. Kramer, Physica D **115**, 19 (1998).

[15] H. Amm, R. Stannarius, and A. Rossberg, Physica D **126**, 171 (1999).

[16] E. F. Carr, J. Chem. Phys. **38**, 1536 (1963); **39**, 1979 (1963); **42**, 738 (1969); Mol. Cryst. Liq. Cryst. **7**, 253 (1969); W. Helfrich, J. Chem. Phys. **51**, 4092 (1969).

[17] Orsay Liq. Cryst. Group, Phys. Rev. Lett. **26**, 1642 (1970).

[18] E. Dubois-Violette, P. G. de Gennes, and O. Parodi, J. Phys. (Paris) (Paris) **32**, 305 (1971).

[19] I. W. Smith, Y. Galerne, S. T. Lagerwall, E. Dubois-Violette, and G. Durand, J. Phys. (Paris), Colloq. **C1**, 237 (1975).

[20] S. Kai, K. Yamaguchi, and K. Hirakawa, Jpn. J. Appl. Phys., Part 1 , Pt. 1 **14**, 1653 (1975).

[21] H. Yamazaki, S. Kai, and K. Hirakawa, J. Phys. Soc. Jpn. **56**, 502 (1987).

[22] L. K. Vistin, A. Yu. Kabaenkov, and S. S. Yakovenko, Kristallografiya **26**, 131 (1981) [Sov. Phys. Crystallogr. **26**, 70 (1981)].

[23] K. Kondon, A. Fukuda, and E. Kuze, Jpn. J. Appl. Phys., Part 1 , Pt. 1 **20**, 1779 (1981).

[24] K. Kondo, A. Fukuda, E. Kuze, and M. Arakawa, Jpn. J. Appl. Phys., Part 1 , Pt. 1 **22**, 394 (1983).

[25] I. Rehberg, F. Horner, and G. Hartung, J. Stat. Phys. **64**, 1017 (1991).

[26] J. A. Kosmopoulos and H. M. Zenginoglou, Appl. Opt. **26**, 1714 (1987).

[27] A. Joets and R. Ribotta, Opt. Commun. **107**, 200 (1994); J. Phys. I **4**, 1013 (1994).

[28] H. Amm, M. Grigutsch, and R. Stannarius, Z. Naturforsch. A **53a**, 117 (1998).

[29] H. Amm, M. Grigutsch, and R. Stannarius, Mol. Cryst. Liq. Cryst. Sci. Technol., Sect. A **320**, 11 (1998).
[30] S. Faetti, L. Fronzoni, and P. Rolla, J. Chem. Phys. **79**, 1427 (1983); S. Faetti and P. Rolla, *ibid.* **79**, 5054 (1983).
[31] S. W. Morris, J. R. de Bruyn, and A. D. May, Phys. Rev. Lett. **65**, 2378 (1990); Phys. Rev. A **44**, 8146 (1991); S. S. Mao, J. R. de Bruyn, and S. W. Morris, Physica A **239**, 189 (1997).
[32] J. J. Wright and J. F. Dawson, Phys. Lett. **43A**, 145 (1973).
[33] L. Nasta, A. Lupu, T. Beica, T. Serban, L. Matei, and M. Giurgea, Mol. Cryst. Liq. Cryst. **53**, 137 (1979).
[34] P. Petrescu and M. Giurgea, Phys. Lett. **59A**, 41 (1976).
[35] D. Igner and J. H. Freed, J. Chem. Phys. **76**, 6095 (1982).
[36] A. Hertrich, A. P. Krekhov, and O. A. Scaldin, J. Phys. II **4**, 239 (1994).
[37] A. Hertrich, dissertation, University of Bayreuth (1996).
[38] S. Akahoshi, K. Miyakawa, and A. Takase, Jpn. J. Appl. Phys., Part 1 , Pt. 1 **15**, 1839 (1976).
[39] H. Miike, Y. Kuriyama, H. Hashimoto, and Y. Ebina, J. Phys. Soc. Jpn. **53**, 3280 (1984).
[40] M. Grigutsch, N. Klöpper, H. Schmiedel, and R. Stannarius, Mol. Cryst. Liq. Cryst. Sci. Technol., Sect. A **262**, 283 (1995).